



The activation/depassivation of nickel–chromium–molybdenum alloys: An oxyanion or a pH effect—Part II



A.K. Mishra^a, D.W. Shoesmith^{a,b,*}

^a Department of Chemistry, University of Western Ontario, London, ON N6A 5B7, Canada

^b Surface Science Western, 999 Collip Circle, London, ON N6G 0J3, Canada

ARTICLE INFO

Article history:

Received 14 February 2013

Received in revised form 28 March 2013

Accepted 28 March 2013

Available online xxx

Keywords:

Nickel alloys

Bicarbonate

Carbonate

pH

XPS

AES

ABSTRACT

The depletion of Cr and Mo in the passive films grown on commercial Ni–Cr–Mo(W) alloys in carbonate/bicarbonate solutions has been studied potentiodynamically and by X-ray photoelectron and Auger spectroscopy. Depletion in these two key alloying elements occurs at lower potentials than expected on all the alloys studied. It has been shown that the key feature leading to this behavior is the buffering of surface pH to >8.6, when the surface deposition (or retention) of insoluble protective Mo(VI) species does not occur as would be expected under the acidic local conditions generated by Cr(VI) and Mo(VI) dissolution. The presence of a small solution concentration of Mg²⁺ ions leads to the accumulation of a Mg(OH)₂ deposit when the surface pH is maintained sufficiently alkaline.

© 2013 Elsevier Ltd. All rights reserved.

1. Introduction

Ni–Cr–Mo alloys having an optimum concentration of Cr and Mo demonstrate excellent corrosion resistance in both oxidizing and reducing environments [1–4]. A Ni–Cr–Mo–W alloy, C-22 (Ni–22Cr–13Mo–3W), has been studied as a candidate material for nuclear waste containers in the proposed Yucca Mountain (Nevada, USA) repository [5]. The exposure conditions under which this alloy may be susceptible to localized corrosion (especially crevice corrosion) have been studied extensively [6–12], with a primary focus on the acidic conditions likely to prevail within an active crevice. In the last ten years many studies have been performed to understand the influence of various parameters, such as, pH, potential and temperature, on the passive film behavior of Ni–Cr–Mo alloys [2,3,10,13–16]. However, the effects of solution composition have not been studied in detail.

In Part I of this study [17] it was demonstrated that, in the presence of bicarbonate ions, the passive film on the Hybrid-BC1 alloy undergoes barrier layer degradation at an unexpectedly low potential. Electrochemical studies show that when the potential is increased above this apparent breakdown value, an anodic peak,

followed by a secondary passive region is observed. It was shown that this film degradation did not result in localized corrosion. X-ray photoelectron spectroscopy (XPS) analyses of the oxide film demonstrated that, in the passive region prior to apparent breakdown potential, the film possesses the expected bilayer structure with a Cr(III)-dominated barrier layer containing mixed oxidation states of Mo and an outer dominantly hydroxide layer. However, at potentials more positive than the apparent breakdown value the Cr/Mo content of the film decreases significantly and the alloy becomes covered by a thick (>100 nm), and only partially protective, Ni(OH)₂ layer in the secondary passivation region.

Recently, Zadorozne et al. [18] showed that this anodic activation in bicarbonate solutions was not limited to Ni–Cr–Mo alloys, but also observed for alloy 800H (Ni–21Cr–45Fe) and alloy 600 (Ni–16Cr–9Fe). However, such an anodic activation was not observed for alloy 201 (Ni–0.1Fe), which does not contain any Cr. These results suggested that the presence of an anodic peak and a secondary passivation region are generic for Cr-containing Ni-based alloys in bicarbonate/carbonate solution.

This study was performed to gain a better understanding of this apparent breakdown process since other authors [19–21] have noted that this activation could render these alloys susceptible to SCC. The effects of parameters, such as alloy composition, pH and temperature were studied using several electrochemical and surface characterization techniques.

* Corresponding author at: Department of Chemistry, University of Western Ontario, London, ON N6A 5B7, Canada. Tel.: +1 519 661 2111x86366.

E-mail addresses: dwshoesm@uwo.ca, ajitosu@gmail.com (D.W. Shoesmith).

Table 1
Nominal chemical compositions of the relevant alloys (wt.% of major alloying element).

Alloying element	C-22 UNS N06022	Hybrid-BC1 UNS N10362	Alloy 59 UNS N06059	Alloy 625 UNS N06625	Alloy 686 UNS N06686
Cr	22	15	23	21	21
Mo	13	22	16	9	16
W	3	–	–	–	4
Fe	3	<2	<1	5	1
Ni	56	62	59	62	58

2. Experimental

2.1. Electrode and solution preparation

Cubic specimens of the alloys 625, C-22, Hybrid-BC1, 59 and 686, with a total surface area of 14.06 cm² were cut from plate material supplied by Haynes International (USA) (625, C-22 and Hybrid-BC1), Thyssenkrupp (USA) (59), and Special Metals (USA) (686). The alloy compositions are given in Table 1. A small tapped hole was machined in the top of the specimen to enable contact to a cylindrical rod. This connector to the external circuit was sheathed in glass and sealed with a teflon gasket to prevent contact with the electrolyte. These electrodes were polished with a series of wet silicon carbide paper up to 1200 grit, rinsed with deionized water and acetone, and air dried prior to an experiment. The specimen was 3/4th (~10 cm²) immersed in the electrolyte to avoid the possibility of a crevice site at the teflon/specimen interface. A platinum foil was used as the counter electrode and the reference electrode was a saturated calomel electrode (SCE).

A standard jacketed, three-electrode cell was connected to a water circulating thermostatic bath allowing control of the solution temperature to within 1 °C. The reference and counter electrodes were housed in separate compartments attached to the main body of the glass cell through glass frits. The cell was placed in a Faraday cage to reduce external sources of electrical noise. Experiments were conducted in 1 M NaCl solution, 0.1 M NaHCO₃ solution, 1 M NaCl + 0.1 M NaHCO₃ solution, 1 M NaCl + 0.1 M Na₂CO₃ solution, 1 M NaCl + 0.01 M Na₂B₄O₇ solution and 1 M NaCl with the pH adjusted by adding various amounts of 0.01 M NaOH solution. Solutions were prepared with Type 1 water (resistivity of 18.2 MΩ cm⁻¹, obtained from a Milli-Q Millipore system) and reagent grade chemicals. The solution was deaerated with Ar throughout an experiment. A fresh solution was prepared for each experiment and all experiments were reproduced at least twice. The temperature of the chloride/bicarbonate solution was varied from 30 to 75 °C but fixed at 60 °C when studying the influences of other parameters. The pH of each solution was recorded before and after an experiment.

2.2. Electrochemical methods

The corrosion potential (E_{corr}) was recorded for 1 h before a polarization experiment. Potentiodynamic scans were performed from ~250 mV below E_{corr} to 800 mV (vs SCE) at a scan rate of 0.167 mV/s. Oxide films for surface analyses were grown by scanning the potential from E_{corr} to the desired potential value at which it was then fixed for 9 h. A slow scan to the film growth potential was used to avoid the initial surge in current observed when a potential step is applied. No cathodic cleaning was performed before any electrochemical experiment.

2.3. Characterization techniques

Electrodes anodically oxidized for surface analyses were rinsed gently with DI water and air dried prior to characterization. XPS

analyses were performed with a Kratos Axis Ultra XPS at Surface Science Western (SSW) employing monochromatic Al K α (1486.8 eV) radiation. The binding energy was calibrated to give a Au 4f_{7/2} line position at 83.95 eV. XPS spectra were corrected for charging by taking the C 1s spectrum for adventitious carbon to be at a binding energy of 284.8 eV. Survey spectra were recorded on all samples followed by high resolution XPS spectra for Ni 2p, Cr 2p, Mo 3d, C 1s and O 1s spectral regions. The XPS spectra were analyzed using the commercial CasaXPSTM software.

Auger data were obtained using a PHI 660 Auger electron spectrometer (AES) with an excitation energy of 5 keV. Depth profiles were measured using an Ar⁺ ion sputtering beam. A survey scan was acquired for each sample and during depth profiling the intensity for Ni, Cr, Mo, Mg and O were monitored as a function of sputtering time. To convert sputtering times to analyzed depths, a reference sputtering profile was obtained on a specimen of the Hybrid-BC1 alloy under similar conditions. The sputtering rate obtained for this reference specimen was 28 nm/min. It was assumed that the sputtering rate for a surface covered with an electrochemically grown oxide was similar to that of the reference specimen.

3. Results

3.1. Effect of alloying elements

Fig. 1 shows the potentiodynamic scans recorded on different alloys in a 1 M NaCl + 0.1 M NaHCO₃ (pH = 8.2) solution at 60 °C. Despite the differences in Cr, Mo and W content of these alloys, they all exhibit similar polarization behavior, the current increasing at $E > 200$ mV (vs SCE) leading to a current peak around ~400 mV followed by a region of secondary passivation prior to complete

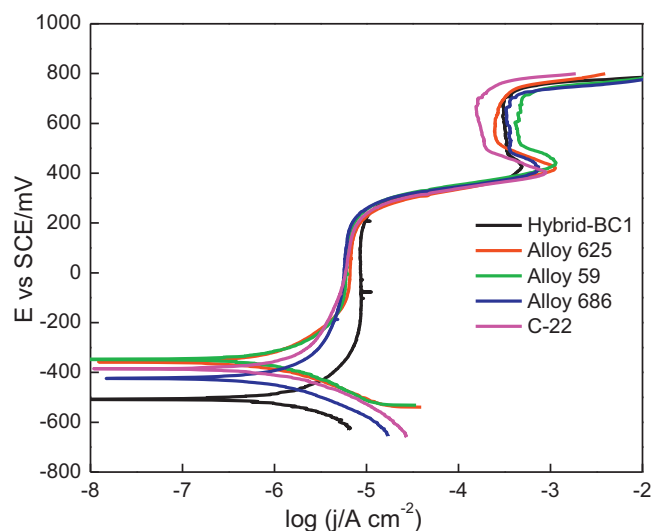


Fig. 1. Potentiodynamic scans recorded on different Ni–Cr–Mo (W) alloys in 1 M NaCl + 0.1 M NaHCO₃ solution at 60 °C.

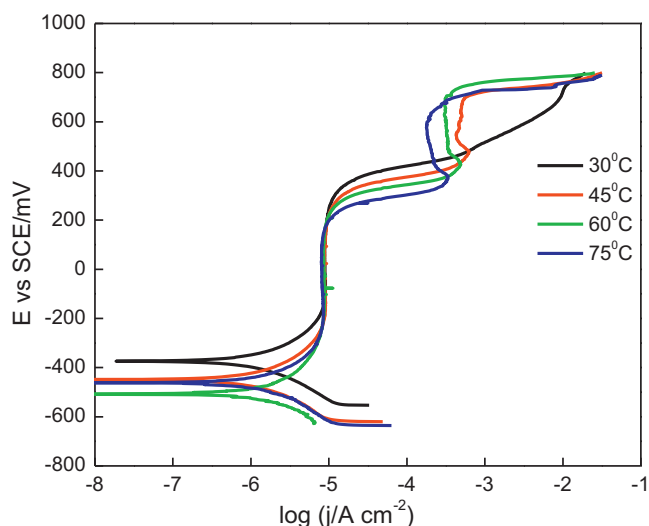


Fig. 2. Potentiodynamic scans recorded on the Hybrid-BC1 alloy in 1 M NaCl + 0.1 M NaHCO₃ solution at different temperatures.

transpassive behavior at potentials above ~ 750 mV. The Hybrid-BC1 alloy has a higher passive current and lower E_{CORR} value than the other alloys, which probably reflects the lower Cr content of this alloy and the relatively short period on open circuit before applying the potentiodynamic scan. However, irrespective of composition, all these alloys exhibit an identical apparent breakdown potential and similar anodic peak potential (425 mV) values.

The similarity in barrier layer degradation potentials, irrespective of compositional differences, indicates that the increase in current beyond the apparent breakdown potential is not a result of localized corrosion. This was demonstrated for the Hybrid-BC1 alloy using cyclic potentiodynamic polarization studies in Part I of the study [17]. Since the passive layer composition on these alloys is likely to be very similar it is not surprising that the potential at which the onset of this barrier layer degradation process commences is independent of the substrate alloy composition. It is anticipated, as previously demonstrated for the Hybrid-BC1 alloy in chloride/bicarbonate solution, that above the apparent breakdown potential all the studied alloys form a thick Ni oxide/hydroxide layer depleted in Cr, Mo and W, which accounts for the secondary partial passivation in the potential range 400–750 mV. These results confirm that the apparent breakdown and the appearance of an anodic peak are independent of the concentration of Cr, Mo or W and other minor alloying elements. Similar behavior for different commercially available Cr-containing Ni-based alloys has been reported by others [18].

3.2. Effect of temperature

The effect of temperature on the polarization curve recorded on the Hybrid-BC1 alloy in 1 M NaCl + 0.1 M NaHCO₃ solution is shown in Fig. 2. At 30 °C, while an increase in current is observed for potentials ≥ 350 mV, no secondary passivation stage is observed at higher potentials. As the temperature is increased, the film degradation potential decreases substantially, the current increase leading to a slight peak followed by a secondary passivation stage as observed for the individual alloys (Fig. 1). The current in this secondary stage decreases with increasing temperature but the final onset of complete transpassivity at potentials ≥ 750 mV is not temperature-dependent.

Zhang [22] previously investigated the influence of temperature on the structure and composition of the passive film on the Ni–Cr–Mo C2000 alloy (23Cr16Mo1.6Cu (wt.%) in chloride solution

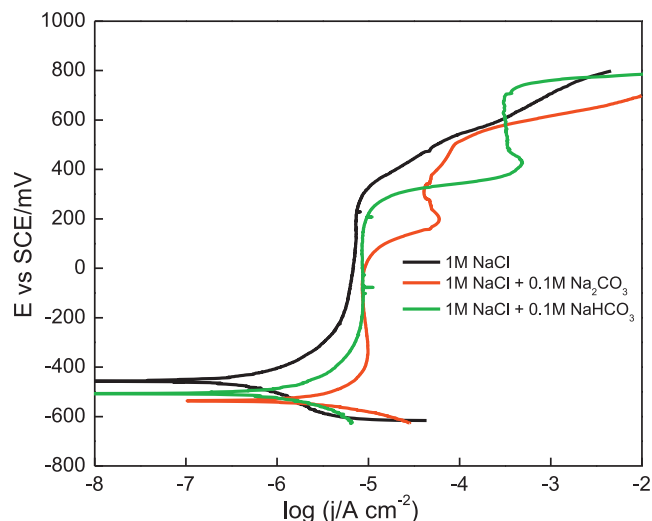


Fig. 3. Potentiodynamic scans recorded on the Hybrid-BC1 alloy in 1 M NaCl, 1 M NaCl + 0.1 M Na₂CO₃ and 1 M NaCl + 0.1 M NaHCO₃ solution at 60 °C.

not containing bicarbonate. Based on XPS and secondary ion mass spectrometry (TOF-SIMS), they demonstrated that an increase in Ni and decrease in Cr/Mo content occurred as the temperature increased at potentials in the passive region. At the potential applied in these studies (0 mV (SCE)) this overall loss of Cr/Mo was offset by an increase in the Cr₂O₃ content of the inner oxide layer. It was claimed that these counterbalancing influences accounted for the absence of any significant influence of temperature on the passive current density. However, in Part I of this study, it was shown that once the potential exceeded the value at which Cr^{III} \rightarrow Cr^{VI} oxidation became possible (i.e., above the apparent breakdown potential observed in this study), then the presence of bicarbonate lead to a rapid loss of Cr and Mo and the formation of a predominantly Ni(OH)₂ layer. This layer suppressed alloy dissolution but did not completely repassivate the surface. This film is referred to as the secondary passivation layer.

The results in Figs. 1 and 2 show that this oxidative breakdown of the passive layer is independent of alloy composition, but very dependent on temperature. The shift of the apparent breakdown potential to more negative values (Fig. 2) is substantially greater than can be explained by a simple influence of temperature on the thermodynamic conversion of Cr^{III} to Cr^{VI}. This suggests that the critical feature controlling the film degradation process is the kinetics of the Cr^{III}/Cr^{VI}, and, to a lesser degree, Mo^{III/IV}/Mo^{VI}, conversion processes and how these are accelerated in the presence of bicarbonate. Since, previously, the film in the secondary passivation region was shown to be a thicker (~ 100 nm compared to a passive film thickness of ~ 3 –4 nm) porous layer of Ni(OH)₂, the decrease in current with temperature in this region (Fig. 2) indicated the film becomes slightly more compact as the temperature increases.

3.3. Effect of carbonate solution

Fig. 3 compares the polarization curves in chloride (pH=7.3), chloride + carbonate (pH=11.0) and chloride + bicarbonate (pH=8.2) at 60 °C. As expected, based on the pH dependence of the redox equilibria involved, the barrier layer degradation potential shifts to more negative potentials as the pH is increased. The maximum current achieved after breakdown (i.e., the peak current value) is significantly lower in carbonate compared to bicarbonate solution, suggesting either the carbonate or the pH (or both) is/are important in determining the scale of Cr/Mo depletion in the film. It was anticipated that the physical, but not necessarily

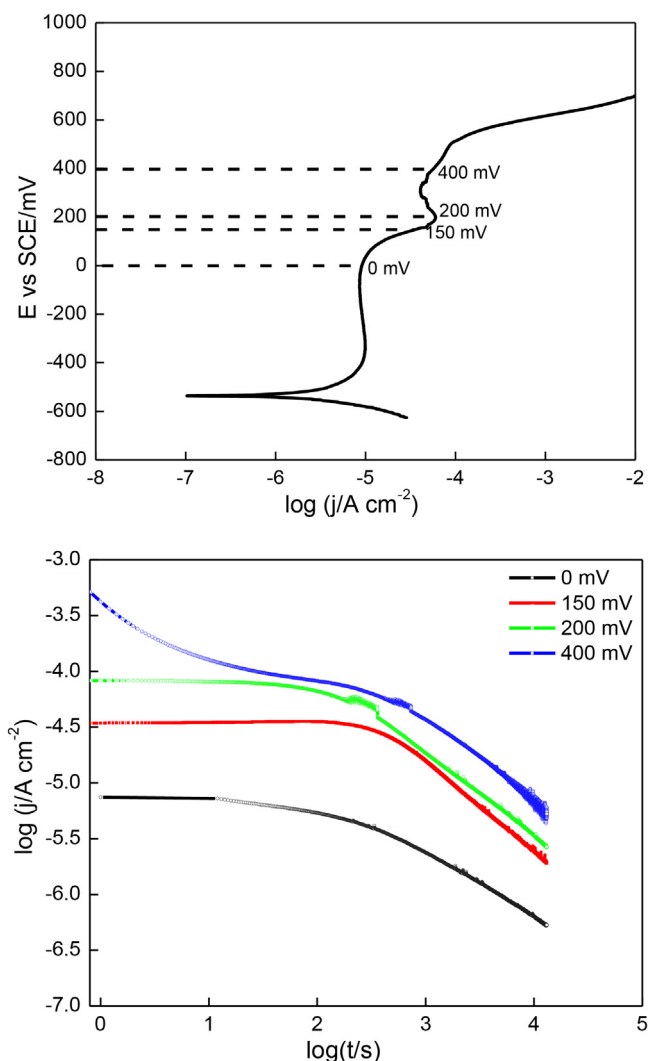


Fig. 4. (a) Potentiodynamic scan recorded on the Hybrid-BC1 alloy in 1M NaCl+0.1M Na₂CO₃ at 60°C showing the potentials at which films were grown. (b) Logarithmic current–time plots recorded at the potentials indicated in (a).

the chemical, properties of the film present in the secondary passivation region are similar for both the solutions (carbonate and bicarbonate).

To confirm that the film formed in the carbonate solution was chemically similar to that formed in bicarbonate solution, a series of potentiostatic film growth experiments followed by XPS and AES analyses were performed, in a similar manner to those performed on oxidized specimens in the bicarbonate solution [17]. The log (current) – log (time) plots recorded at potentials in the passive region (0 mV), in the increasing current region (150 mV), at the peak (200 mV) and in the secondary passivation region (400 mV) are shown in Fig. 4.

The general form of these curves is similar to those recorded in the chloride/bicarbonate (pH=8.2) solution and has been discussed previously [17]. The decreasing current observed over the log time interval 2 to >4 (Fig. 4b) is consistent with the development of a partially passivating surface film. The final currents are up to two orders of magnitude less than those observed at these potentials in the polarization curves (Fig. 4a) and still decreasing. This indicates that the film present, even in the secondary passivation region, is sufficiently resistive to partially protect the alloy.

To confirm that the composition of films grown in chloride/carbonate (pH=11.0) solution is the same as that of films

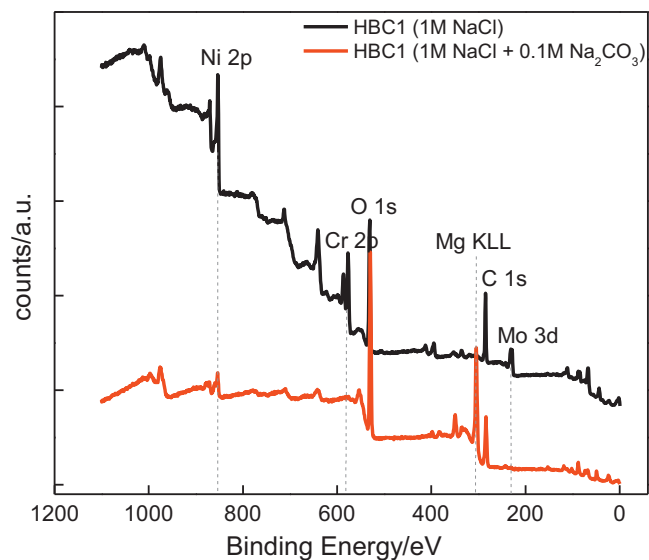


Fig. 5. XPS survey spectra for the films grown at 0 mV (SCE) in chloride and chloride/carbonate solution.

grown in chloride/bicarbonate (pH=8.2) solutions [17], XPS and AES analyses were conducted on the potentiostatically grown films. Fig. 5 shows XPS survey spectra recorded at 0 mV (in the passive region) in chloride (pH=7.3) and chloride/carbonate (pH=11.0) solutions. As indicated by the dashed vertical lines Ni-2p, Cr-2p and Mo-3d peaks are clearly visible after anodic oxidation in the chloride solution. However, after oxidation in the chloride/carbonate (pH=11.0) solution neither Cr nor Mo is detected and the Ni peak is significantly reduced in height. In addition, a strong Auger peak for Mg (Mg-KLL) is observed when carbonate is present. The high background signal observed in the absence of carbonate can be attributed to the very high yield of emitted photoelectrons from the base alloy which experience energy loss when only a thin passive oxide is present. The considerably lower background emission when Mg is present suggests this photoelectron yield is limited by the presence of a surface layer of Mg oxide/hydroxide.

Fig. 6 compares the current–time plot for anodic oxidation at 0 mV in the chloride/carbonate (pH=11.0) solution to that obtained at the same potential in chloride/bicarbonate (pH=8.2) solution

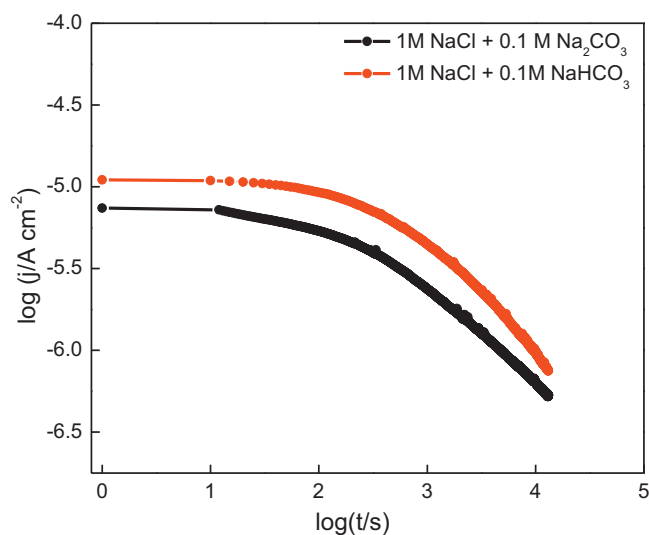


Fig. 6. Log(*I*) – log(*t*) plots recorded on the Hybrid-BC1 alloy in chloride/carbonate and chloride/bicarbonate solution at 0 mV (SCE).

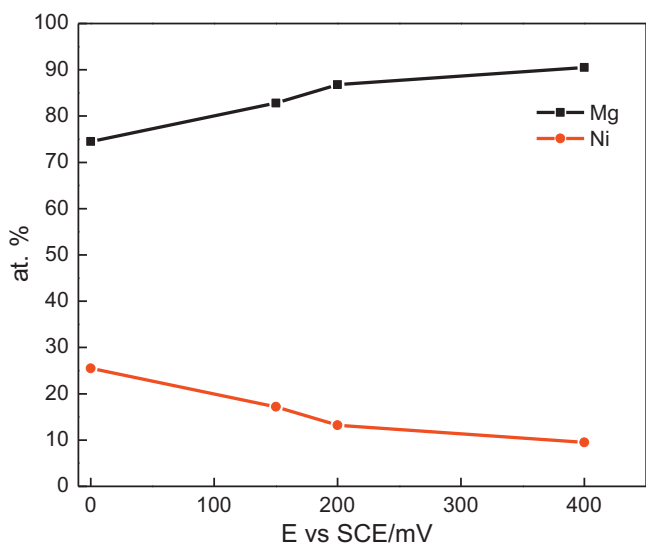


Fig. 7. Film cation composition as a function of potential recorded on the Hybrid-BC1 alloy in 0.1 M NaCl + 0.1 M Na₂CO₃ solution.

[17]. In both solutions, this potential is well within the passive region and the currents, as well as their evolution with time, are very similar. Considering this similarity, depletion of the passive film in Cr/Mo would not be expected at 0 mV.

Fig. 7 shows the cation fractions in the surface of the film as a function of applied potential in the chloride/carbonate (pH = 11.0) solution. Only Ni and Mg are observed over the whole potential range. The fraction of Mg increases with increasing potential. High resolution spectra for Ni-2p (not shown), using the fitting parameters determined by Biesinger et al. [23,24], show that the Ni film present in the secondary passivation region is predominantly Ni(OH)₂ with small amount of NiO as observed previously in the chloride/bicarbonate (pH = 8.2) solution [17]. An Auger depth profile recorded on the electrode anodically oxidized at 200 mV, Fig. 8, shows that the film is multilayered with an Mg(OH)₂ layer on the outer surface and an Ni(OH)₂ layer at the oxide/alloy interface. This profile suggests that, while depleted in the outer regions of the film, some Cr and Mo may still be present at the alloy/film interface.

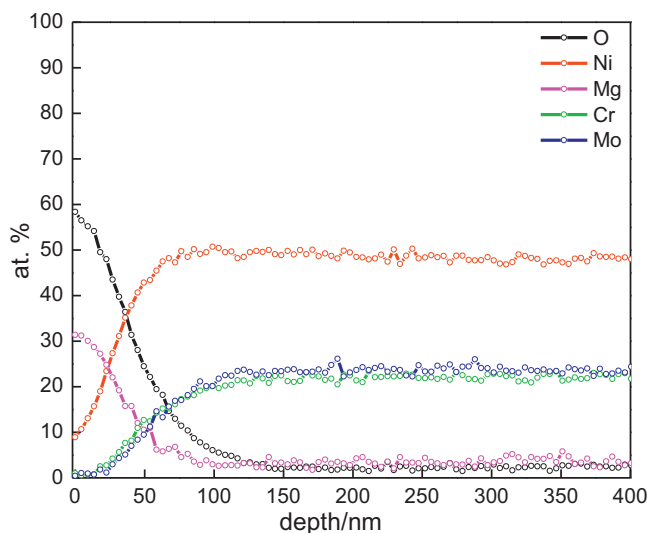


Fig. 8. AES depth profile recorded on the Hybrid BC1 alloy after anodic film growth at 200 mV (Fig. 4a) in 1 M NaCl + 0.1 M Na₂CO₃ solution.

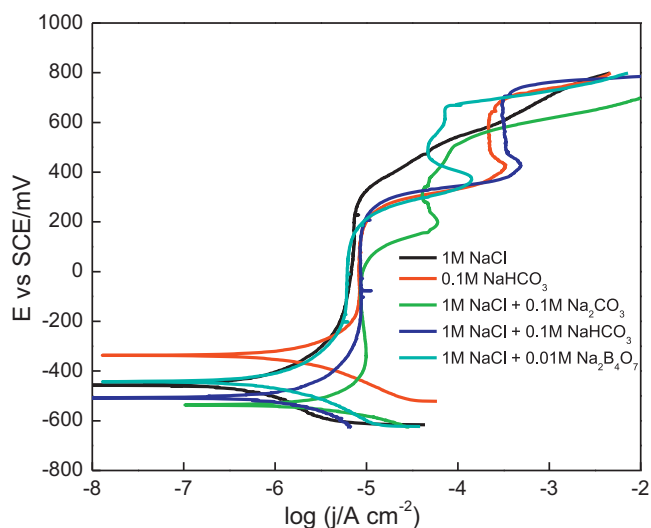


Fig. 9. Potentiodynamic scan recorded on the Hybrid-BC1 alloy in different solutions at 60 °C.

If the depth at which the O signal in the Auger profile reaches half its surface value is taken as the location of the oxide alloy interface, then an overall thickness of ~45 nm is obtained for the film at this potential. This compares to a thickness of ≥ 100 nm in chloride/bicarbonate (pH = 8.2) solution reported in Part I [17]. This decrease in thickness suggests that the accumulation of this outer layer suppresses the overall extent of film formation/alloy dissolution. The presence of a similar layer of Mg(OH)₂ in the passive region (0 mV), Fig. 7, would account for the inability to detect Cr and Mo in the thin passive film by XPS.

The only source of Mg ions in the system is the impurity content of the Na₂CO₃ salt used to prepare the solution. If the Mg is present at the maximum impurity level then the calculated concentration present in our solution should be $< 5 \times 10^{-6}$ mol/L. Given a solubility product of $\sim 10^{-11}$ mol²/L² for Mg(OH)₂, its accumulation on the electrode surface would be possible at pH = 11.0. While this would account for the presence of Mg(OH)₂ on the alloy surface it would not explain its increasing dominance on the surface as the potential is made more positive (Fig. 7) and the anodic current increases (Fig. 3).

3.4. Effect of buffering anions

Fig. 9 shows polarization scans recorded on the Hybrid-BC1 alloy in the 1 M NaCl (pH = 7.3), 0.1 M NaHCO₃ (pH = 8.3), chloride/carbonate (pH = 11.0), chloride/bicarbonate (pH = 8.2) and chloride/borate (pH = 8.8) solutions. Comparison of the behavior in the chloride, bicarbonate and chloride/bicarbonate solutions shows that the influence of chloride is insignificant and confirms that the transition with potential from the primary (<200 mV) to the secondary (>400 mV) passivation regions is due to the presence of bicarbonate/carbonate. However, similar behavior to that observed in the bicarbonate and chloride/bicarbonate is observed also in the chloride/carbonate and chloride/borate solution. The graph shows that with an increase in pH, the maximum current (at the peak) and the current in the secondary passivation region decrease substantially. These results confirm that the nature of the anion (bicarbonate, carbonate or borate) is not the key feature determining the current increase leading to Cr/Mo depletion. Although not shown, similar behavior was observed for alloy 59.

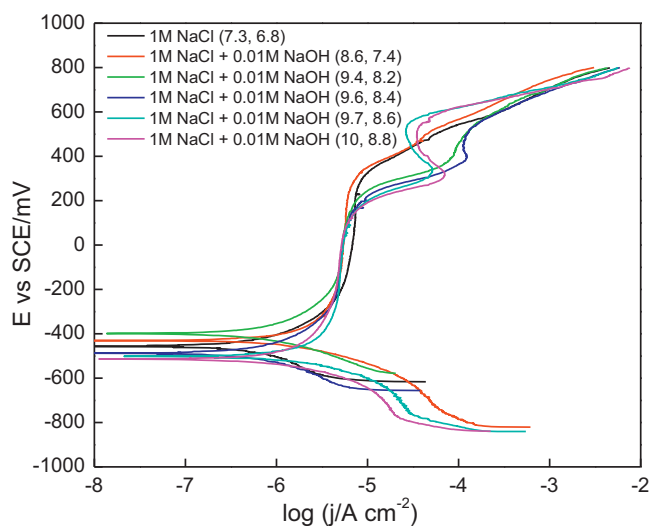


Fig. 10. Potentiodynamic scans recorded on the Hybrid-BC1 alloy at 60 °C in chloride/hydroxide solutions containing various amounts of added NaOH. The pH values measured before and after the experiments are shown in brackets.

3.5. Effect of hydroxide

To determine whether the pH is the critical influence in the anodic process leading to Cr/Mo loss from the passive film, a series of experiments was performed in 1 M NaCl + 0.01 M NaOH. The solution pH was adjusted by increasing the volume of added NaOH. The potentiodynamic scans, Fig. 10, show that increasing the pH sufficiently also leads to the appearance of the anodic peak/secondary passivation region. As indicated in the figure, the pH of the bulk solution decreases, since the loss of Cr and Mo by dissolution of the passive film and the transpassive dissolution of the alloy will produce a considerable number of protons. Since, most of the bulk solution pH change observed will have occurred during the transpassive dissolution process, the relevant pH defining the behavior in the passive/secondary passivation regions (i.e., whether or not anodic activation leading to Cr/Mo loss occurs) is the initial bulk solution pH. Based on Fig. 10, the threshold pH is in the range 8.6–9.4. The pH values after polarization are predominantly due to the very high currents in the transpassive region and do not represent the pH value prevailing as the scan passes through the anodic peak/secondary passivation region.

3.6. Buffered and unbuffered solutions

The maximum current corresponding to the anodic peak is considerably smaller in chloride/hydroxide solution (pH – 8.6) compared to that of the chloride/bicarbonate solution (pH – 8.2) (Fig. 11) possibly due to the incomplete depletion of Cr/Mo in the former case. To determine whether this is the case, films grown in the two solutions, at a potential of 335 mV (SCE) in chloride/hydroxide solution and 425 mV (SCE) in chloride/bicarbonate solution, were analyzed by XPS. The survey spectra show that both Cr and Mo are undetectable in both cases, and Fig. 12, which shows the high resolution deconvoluted Ni-2p spectra for both films are very similar, confirms that the film composition is dominantly Ni(OH)₂. These analyses confirm that the large differences in measured anodic currents are not due to differences in film composition. Since the chloride/hydroxide solution is unbuffered, it seems likely that the lower anodic current is related to a decrease in surface pH, sufficient to reduce the solubility of oxidized Cr and Mo species, but not sufficiently to prevent their depletion in the film.

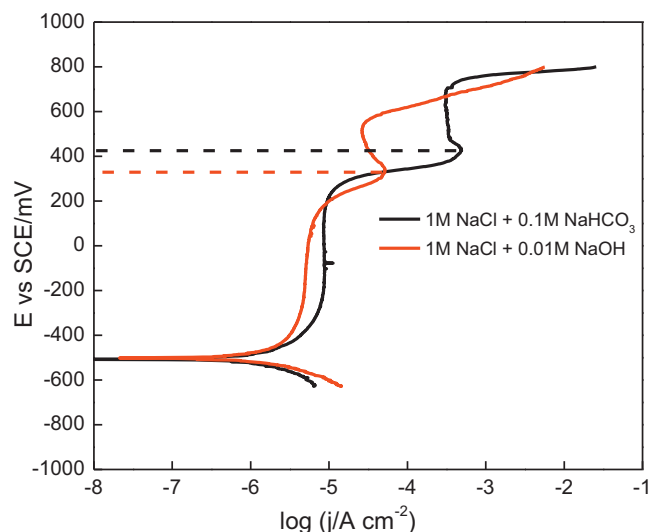


Fig. 11. Potentiodynamic scans recorded on the Hybrid-BC1 alloy at 60 °C in chloride/bicarbonate and chloride/hydroxide solutions. The horizontal dashed lines show the potentials at which films were grown and analyzed by XPS.

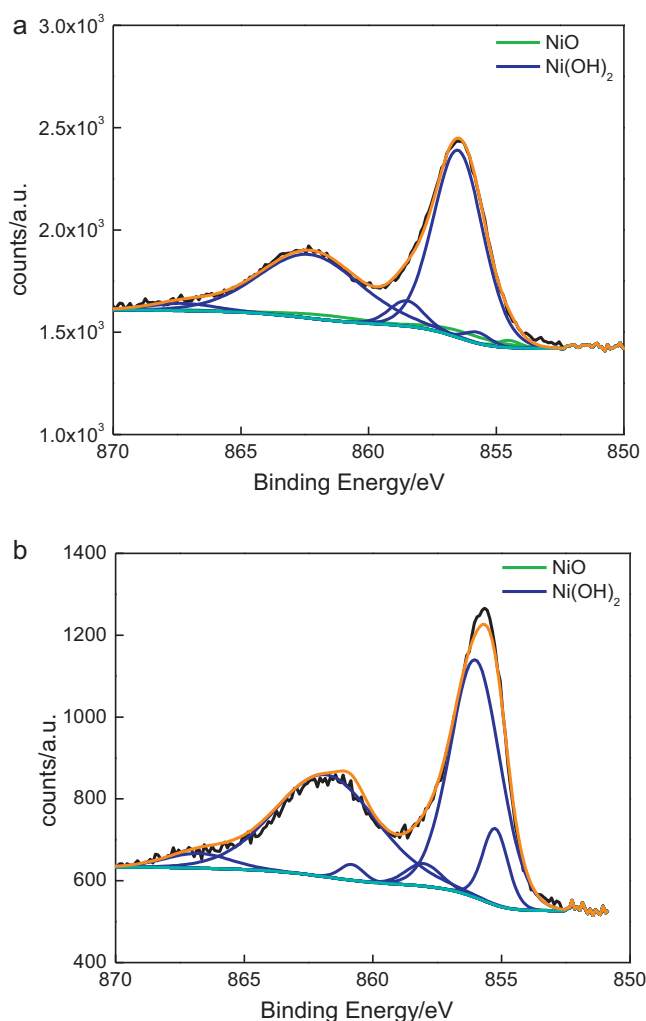
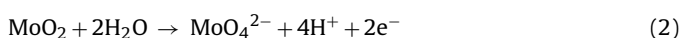


Fig. 12. High resolution deconvoluted XPS spectra for the Ni 2p peak recorded on oxide films grown on the Hybrid-BC1 at 60 °C at a potential of 335 mV (SCE) and 425 mV (SCE) (Fig. 11) in (a) chloride/hydroxide solution and (b) chloride/bicarbonate solution respectively.

4. Discussion

Previous electrochemical impedance spectroscopy and XPS measurements connected the onset of passive film breakdown to the start of the anodic destruction of the Cr(III) oxide-dominated barrier layer to yield the more soluble CrO_4^{2-} . XPS and time-of-flight secondary ion mass spectrometry (ToF-SIMS) also showed [13,15,16] that this breakdown was accompanied by the creation of oxidized states of Mo(VI) and W(VI) and it has been proposed that the retention of these latter states in the outer regions of the passive film extends the passive region to considerably higher potentials [3,15,17]. The segregation of oxidized Mo/W states to the outer regions of the film and the maintenance of passivity is particularly well marked under acidic conditions [3] when the solubility of molybdates (and tungstates) is minimized.

Even under neutral pH conditions any attempt to oxidize the Cr(III) barrier layer and the Mo(II,III,IV) species within the passive film [16] will generate local acidity via the reactions



facilitating the deposition of protective molybdates within the outer regions of the film and the maintenance of passivity to more positive potentials. The structure of the molybdates present in the passive surface remains uncharacterized but it is well known that acidic conditions are required to generate the polymeric species known to exist in gel-like structures [8].

It is not surprising, therefore, that an increase in pH by the addition of OH^- will neutralize the surface pH and facilitate the dissolution of potentially protective Mo(VI) species as soluble molybdates, MoO_4^{2-} , rather than allow the proton driven deposition of protective molybdates. In the absence of this protective segregated outer layer (a similar argument can be made for tungstates) the release of soluble CrO_4^{2-} by anodic oxidation of the Cr(III) oxide barrier layer would be kinetically uninhibited. This would leave Ni(II) as the only insoluble alloying component leading to the formation of $\text{Ni}(\text{OH})_2$ in the secondary passivation region.

The identification of a critical pH of ~ 8.6 , below which Cr/Mo depletion of the passive film does not occur then explains why the presence of carbonate/bicarbonate and borate also lead to Cr/Mo depletion once the anodic oxidation of the Cr(III) oxide barrier layer commences. These anions act as pH buffers within this pH range maintaining the surface pH above the critical value thereby preventing the local acidification required to precipitate and polymerize Mo(VI) and prevent the rapid anodic destruction of the Cr(III) barrier layer.

It is also possible that this buffering could facilitate the accumulation of $\text{Mg}(\text{OH})_2$ on the alloy surface in the chloride/carbonate solution. Its accumulation in the passive region can only be attributed to the solubility effect but its increase with potential suggests this accumulation is enhanced by the anodic process. All the species formed by the anodic activation process are anionic (e.g., CrO_4^{2-} , MoO_4^{2-}) except for the H^+ . When these protons are absorbed by the carbonate buffer, both the carbonate and bicarbonate are also anions. In the borate case either anions (BO_3^{3-} , HBO_3^{2-} , H_2BO_3^-) or neutral (H_3BO_3) species are formed. As a consequence, the solution in the immediate vicinity of the surface is cation deficient, and the electrical migration of Na^+ and Mg^{2+} to the electrode surface will occur. This will increase the concentration of Mg^{2+} in the vicinity of the surface facilitating $\text{Mg}(\text{OH})_2$ deposition, thereby, accounting for the enhanced accumulation of the $\text{Mg}(\text{OH})_2$ at higher potentials (Fig. 7).

5. Conclusions

- Potentiodynamic scans on a series of commercial Ni–Cr–Mo (W) alloys show an apparent breakdown of the passive film at a lower than expected potential followed by an anodic peak and a secondary passive region. This behavior was only observed in the presence of carbonate/bicarbonate and borate buffers and in alkaline solutions, and was independent of the composition of the alloy.
- Consistent with previous studies, XPS and AES analyses confirmed that the film was depleted in Cr/Mo and covered by a $\text{Ni}(\text{OH})_2$ layer in the secondary passivation region.
- Varying the pH of the solution by adding hydroxide showed that this apparent breakdown/secondary repassivation process required a $\text{pH} > 8.6$ for various commercially available Ni–Cr–Mo (W) alloys in different buffer solutions, like bicarbonate/carbonate and borates. It was also noticed that the apparent breakdown potential and anodic peak potential was independent of the concentration of Ni, Cr, Mo, W and other minor alloying elements.
- The presence of a small concentration of Mg^{2+} in the chloride/carbonate solution leads to the accumulation of a $\text{Mg}(\text{OH})_2$ layer on the electrode surface. While the deposition of this layer can mainly be attributed to the insolubility of the hydroxide, the extent of deposition appears to be accelerated by the depletion of cations near the electrode surface as the protons produced by the anodic dissolution of Cr(VI) and Mo(VI) are buffered into anionic form. To counterbalance this depletion, solution cations including Mg^{2+} , migrate to the electrode surface.

Acknowledgements

This research was funded by the Canadian Natural Sciences and Engineering Research Council (NSERC). The authors also acknowledge Haynes International, ThyssenKrupp and Special Metals for providing the samples. Special thanks go to Dr. Sridhar Ramamurthy and Dr. Mark Biesinger at Surface Science Western (SSW) for their assistance on analytical techniques employed in this study.

References

- [1] W.Z. Friend, *Corrosion of Nickel and Nickel-Based Alloys*, John Wiley and Sons, NY, 1980.
- [2] J.R. Hayes, J.J. Gray, A.W. Szmodis, C.A. Orme, Influence of chromium and molybdenum on the corrosion of nickel-based alloys, *Corrosion* 62 (2006) 491.
- [3] A.C. Lloyd, J.J. Noel, N.S. McIntyre, D.W. Shoesmith, Cr, Mo and W alloying additions in Ni and their effect on passivity, *Electrochimica Acta* 49 (2004) 3015.
- [4] K.J. Evans, A. Yilmaz, S.D. Day, L.L. Wong, J.C. Estill, R.B. Rebak, Using electrochemical methods to determine alloy 22's crevice corrosion repassivation potential, *Journal of Occupational Medicine* 57 (2005) 56.
- [5] G.M. Gordon, Corrosion considerations related to permanent disposal of high-level radioactive waste, *Corrosion* 58 (2002) 811.
- [6] A.K. Mishra, G.S. Frankel, Crevice corrosion repassivation of alloy 22 in aggressive environments, *Corrosion* 64 (2008) 836.
- [7] X. Shan, J.H. Payer, Characterization of the corrosion products of crevice corroded alloy 22, *Journal of Electrochemical Society* 156 (2009) C313.
- [8] P. Jakupi, F. Wang, J.J. Noel, D.W. Shoesmith, Corrosion product analysis on crevice corroded alloy-22 specimens, *Corrosion Science* 53 (2011) 1670.
- [9] P. Jakupi, J.J. Noel, D.W. Shoesmith, Crevice corrosion initiation and propagation on alloy-22 under galvanically-coupled and galvanostatic conditions, *Corrosion Science* 53 (2011) 3122.
- [10] A.C. Lloyd, J.J. Noel, N.S. McIntyre, D.W. Shoesmith, The open circuit ennoblement of alloy C-22 and other Ni–Cr–Mo alloys, *Journal of Occupational Medicine* 57 (2005) 31.
- [11] N.S. Zadorozne, C.M. Giordano, M.A. Rodriguez, R.M. Carranza, R.B. Rebak, Crevice corrosion kinetics of nickel alloys bearing chromium and molybdenum, *Electrochimica Acta* 76 (2012) 94.
- [12] M.R. Ortiz, M.A. Rodriguez, R.M. Carranza, R.B. Rebak, Determination of the crevice corrosion stabilization and repassivation potentials of a corrosion-resistant alloy, *Corrosion* 66 (2010) 1.

- [13] A.C. Lloyd, D.W. Shoesmith, N.S. McIntyre, J.J. Noel, Effects of temperature and potential on the passive corrosion properties of alloy C22 and C276, *Journal of Electrochemical Society* 150 (2003) B120.
- [14] P. Jakupi, D. Zagidulin, J.J. Noel, D.W. Shoesmith, The impedance properties of the oxide film on the Ni–Cr–Mo alloy 22 in neutral concentrated sodium chloride solution, *Electrochimica Acta* 56 (2011) 6251.
- [15] X. Zhang, D. Zagidulin, D.W. Shoesmith, Characterization of film properties on the Ni–Cr–Mo alloy C-2000, *Electrochimica Acta* 89 (2013) 814.
- [16] D. Zagidulin, X. Zhang, J. Zhou, J.J. Noel, D.W. Shoesmith, Characterization of surface composition on alloy 22 in neutral chloride solutions, *Surface and Interface Analysis*, in press, <http://dx.doi.org/10.1002/sia.5204>
- [17] A.K. Mishra, S. Ramamurthy, M. Biesinger, D.W. Shoesmith, The activation–depassivation of nickel–chromium–molybdenum alloys in bicarbonate solution: Part I, *Electrochimica Acta*, in press, <http://dx.doi.org/10.1016/j.electacta.2013.03.161>
- [18] N.S. Zadorozne, R.M. Carranza, M.C. Giordano, A.E. Ares, R.B. Rebak, Effect of temperature and chloride concentration on the anodic behavior of nickel alloys in bicarbonate solutions, *Corrosion*, Paper No. 0001413, NACE, Salt Lake City, UT, March 11–15, 2012.
- [19] K.T. Chiang, D.S. Dunn, G.A. Cragnolino, Effect of simulated groundwater chemistry on stress corrosion cracking of alloy 22, *Corrosion* 63 (2007) 940.
- [20] J.C. Estill, K.J. King, D.V. Fix, D.G. Spurlock, G.A. Hust, S.R. Gordon, R.D. McCright, G.M. Gordon, R.B. Rebak, Susceptibility of alloy 22 to environmentally assisted cracking in Yucca Mountain relevant environments, *Corrosion*, Paper No. 02535, NACE, Denver, CO, April 7–12, 2002.
- [21] K.J. King, L.L. Wong, J.C. Estill, R.B. Rebak, Slow strain rate testing of alloy 22 in simulated concentrated ground waters, *Corrosion*, Paper No. 04548, NACE, New Orleans, LA, March 28–April 1, 2004.
- [22] X. Zhang, Ph.D. Thesis, Department of Chemistry, University of Western Ontario, London, ON, 2012.
- [23] M.C. Biesinger, B.P. Payne, L.W.M. Lau, A.R. Gerson, R.S. Smart, X-ray photoelectron spectroscopic chemical state quantification of mixed nickel metal, oxide and hydroxide systems, *Surface and Interface Analysis* 41 (2009) 324.
- [24] M.C. Biesinger, B.P. Payne, A.P. Grosvenor, L.W.M. Lau, A.R. Gerson, R.S. Smart, Resolving surface chemical states in XPS analysis of first row transition metals, oxides and hydroxides: Cr, Mn, Fe, Co and Ni, *Applied Surface Science* 257 (2011) 2717.